ADVANCED MATERIALS TECHNOLOGIES

www.advmattechnol.de

An Electrically Renewable Air Filter with Integrated 3D Nanowire Networks

Kai Yang, Zhihao Yu, Changcheng Yu, Haibiao Chen, and Feng Pan**

Particulate matter (PM) is a major pollutant in air and filtration at the source and on-site is an effective approach to remedy PM pollution. Filters integrated with nanowires are advantageous for their high PM removal efficiency and low resistance to airflow. In this work, carbon nanowires are directly grown as 3D networks on a 304 stainless steel mesh to form a robust air filter. The growth of the carbon nanowires is initiated by exposing the stainless steel substrate to the vapor generated from the thermal decomposition of a silicone. The stainless steel is attacked by the carbon supersaturated vapor and releases metal nanoparticles, which catalyze the growth of carbon nanowires. The air filter with integrated 3D nanowire networks achieves a high PM removal efficiency with a low pressure drop. Moreover, the filter is heat resistant and can be renewed by electrical resistive heating to burn off the captured PM. After electrical renewal treatment, the filter recovers the low pressure drop while still maintaining a high PM removal efficiency. This air filter is promising for applications requiring on-site renewal and will be useful for treating high temperature emissions.

1. Introduction

Air pollution has become a global issue due to the lack of awareness of the environment during the rapid development of industry and economy for ages.[1] As one of the major pollutants in the atmosphere, particulate matter (PM) has adverse effects on human health, ecosystem, and visibility.[2] PM can be described using its "aerodynamic equivalent diameter" (AED),[2a] and particles of the similar AED tend to have the same settling velocity. PM is traditionally classified into three categories:[2a,c] coarse particles (AED > 2.5 μm), fine particles (AED = 0.1–2.5 μm), and ultrafine particles (AED < 0.1 μm). $PM_{2.5}$ refers to PM with an AED smaller than 2.5 μm. Compared with coarse particles, $PM_{2.5}$ tends to carry more toxic organics, heavy metals, and harmful microorganisms because of its higher specific surface area and more active sites.[2a]

Sources of PM include both natural and anthropogenic. Natural sources include sandstorms, volcanos, and wildfires. Anthropogenic sources include industrial waste gases, vehicle emissions, urban fugitive dusts, and volatile organic pollutions.[1–3] Generally, source control and air purification are two main approaches to remedy the PM pollution. Source control is a long-term process, and governments from all over the world have established regulations to reduce PM emission. Air purification can be efficient and timesaving, and researchers have developed different methods and materials to capture PM.

PM can be captured using filtration materials. The structure of typical commercial filters can be classified as either porous or fibrous as shown in Figure S1 in the Supporting Information. Porous filters are usually prepared by forming pores on solid substrates and the pressure drop across this type of filter is usually high due to low porosity. While in fibrous filters, it is reported that a "slip-flow effect" would arise when the diameter of the fibers is under 500 nm and it reduces the pressure drop.[3,4] Besides, the fibrous filters have a relatively higher specific surface area that could enhance the filtration efficiency at a high structural porosity. Within the category of fibrous filters, fibers with nanometer range diameters would impose even lower resistance to the airflow. Fibrous materials such as carbon nanotubes,[5] carbon nanofibers,[6] silk nanofibers,[7] chitosan nonwovens[8] etc., are widely used in air purification owing to their abundant reserves, physical and chemical stability, high specific surface, hierarchical porous structures, and active adsorption sites. Generally, the filtration mechanism can be either passive or proactive depending on the interaction between the filtration materials and PM.[4,9] In the passive filtration process, PM in motion is captured by the filtration material through collision, attachment, and trapping.[4,9] While in the proactive process, the chemical and electrostatic interactions[10] between PM and the filtration material become effective.[4,9]

Researchers introduced several parameters to evaluate the performance of the filtration materials:[3,4,9] PM removal efficiency, pressure drop, and chemical and thermal stability, etc. Detailed definitions of some parameters are listed in Table S1 in the Supporting Information. Generally, PM removal efficiency represents the ability to filter PM, and pressure drop evaluates the resistance to the airflow. PM removal from high temperature exhaust gas has recently attracted much attention,[6,11] and the thermal stability as well as the oxidation resistance of the filtration materials becomes important. In addition, reducing the life-cycle cost of the materials and the impact to

K. Yang, Z. Yu, C. Yu, Prof. H. Chen, Prof. F. Pan
School of Advanced Materials
Peking University Shenzhen Graduate School
Shenzhen 518055, China
E-mail: chenhb@pkusz.edu.cn; panfeng@pkusz.edu.cn

The ORCID identification number(s) for the author(s) of this article can be found under https://doi.org/10.1002/admt.201900101.

DOI: 10.1002/admt.201900101

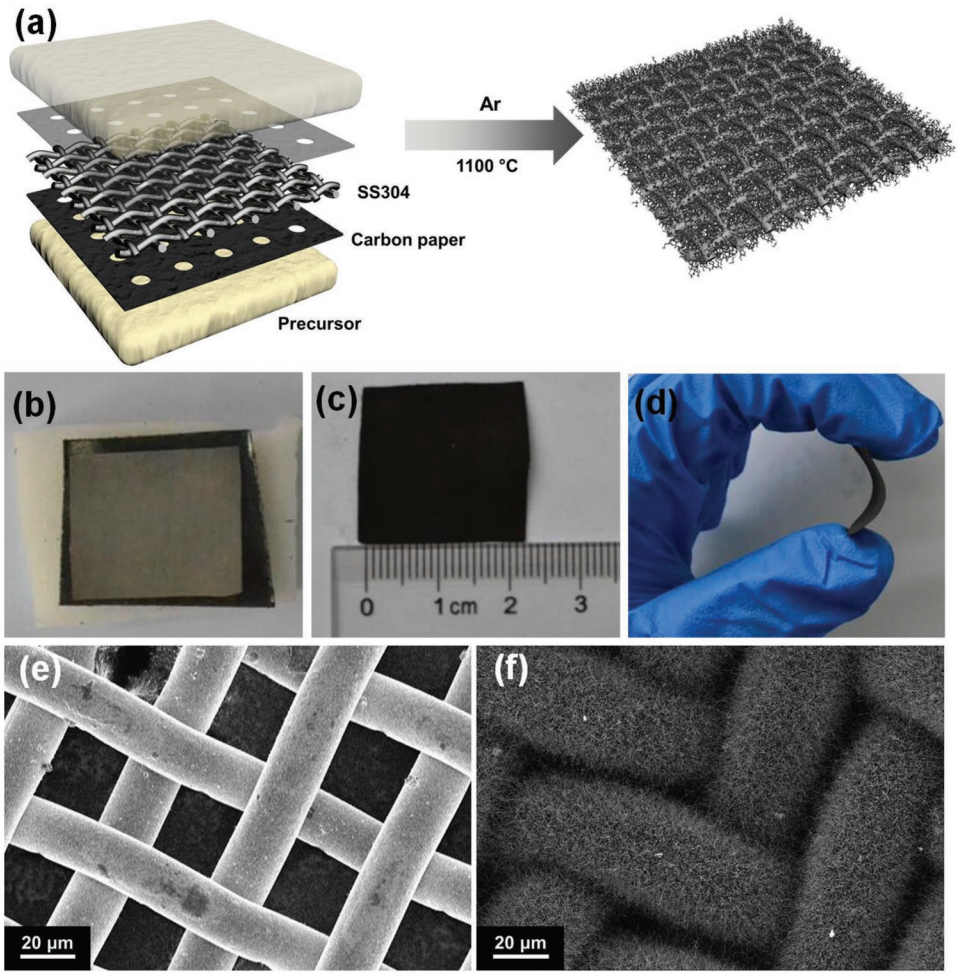

Figure 1. a) Method for growing carbon nanowires on SS304 mesh; b) The SS304 mesh substrate, with carbon paper and silicone underneath; c,d) The SS304 mesh after carbon nanowires grown; e) SEM of SS304 mesh before carbon nanowire growth; f) SEM of SS304 mesh after carbon nanowires grown.

the environment by using sustainable or renewable materials for PM filtering is an eco-friendly strategy for remedying PM pollution.[12] Many commercial filters cannot be regenerated and the filtration material needs to be replaced when it is saturated with PM. Apparently, the capability of being renewable is desirable for reducing the maintenance cost of the filters. In addition, there are scenarios where the filters need to be renewed on-site. Overall, it is of great interest to develop high performance filtration materials that are thermally stable, oxidation resistant, and easily renewable.

In this work, we demonstrate a novel PM filter with networks of carbon nanowires directly grown on a 304 stainless steel (SS304) mesh. Apparently, a filter substrate of a stainless steel material is mechanically robust and heat resistant. The filter achieved a high PM removal efficiency of over 95% and a low resistance to the airflow. The functional groups on the surface of the nanowires contribute to the proactive capturing of the organic components in PM. The filter was heat resistant for certain duration, so it is potentially capable of filtering high temperature gases such as diesel engine exhausts. Moreover, the filter is electrically conductive and a renewal treatment of the filter by electrical resistive heating was demonstrated. The filter can be renewed by burning off the captured PM when a current is fed through and revert to the initial performance.

2. Results and Discussion

2.1. Microstructure of the Carbon Nanowire Networks

The nanowires were grown on the SS304 substrate using an in situ vapor growth method and the overall experimental setup is schematically illustrated in **Figure 1**a,b. Instead of feeding precursor vapors for the reaction, organic vapors were generated in situ by the decomposition of a solid precursor, which is heated in adjacent to the SS304 substrate. The solid organic precursor used in this work was a polysiloxane, which decomposes to produce a mixture of hydrocarbons and silanes upon pyrolysis. Preparation of the silicone precursor involves cross-linking between polymethylhydrosiloxane (PMHS) and RTV 615A as shown in Figure S2a in the Supporting Information. The functional groups on the polymers were identified by Fourier-transform

infrared spectroscopy (FTIR). The Si—H bonds (peaks at 2160 and 910 cm^{-1} in the FTIR spectrum in Figure S2b, Supporting Information)[13] from PMHS reacted with the C=C bonds (peak at 1620 cm^{-1} in the FTIR spectrum in Figure S2b, Supporting Information)[14] from RTV 615A and a solid silicone was produced. FTIR result in Figure S2b (Supporting Information) shows that the cross-linked product contained no Si—H bonds, suggesting the polymerization was complete. The silicone was used as a precursor to generate gaseous hydrocarbons to grow nanowires on the SS304 substrate. After growing carbon nanowires, the color of the mesh changed from metallic silvery to black as shown in Figure 1c. The SS304 mesh with integrated carbon nanowires remained flexible and strong as seen in Figure 1d. Typical structures of the 3D nanowire networks grown on SS304 mesh as observed by a scanning electron microscope (SEM) are shown in Figure 1f and Figure S3 (Supporting Information). The smooth surface of the wires in the SS304 mesh became "hairy" after the carbon nanowires were grown. The heat treatment temperature was found to be crucial in determining the growth of the nanowires. Growth of the carbon nanowire was carried out at different temperatures of 1000, 1050, 1100, and 1200 °C. An optimal growth temperature was selected by evaluating the microstructure of the nanowires using SEM. As shown in Figure S4 (Supporting Information), population of the nanowires grown at 1100 °C was the densest, and the openings (30 μm × 30 μm as shown in Figure 1e) of the SS304 mesh were completely traversed by the nanowire networks. The length of the nanowires is mostly in the range of tens of micrometers.

Detailed microstructure of the nanowire observed by transmission electron microscopy (TEM) is shown in **Figure 2**a,b and Figure S5 (Supporting Information). The diameter of the nanowires was quite uniform and a typical value was ≈120 nm. High-resolution TEM (HRTEM) images in Figure 2b and Figure S5 (Supporting Information) reveal that the core region of the nanowire has a crystalline structure with a fringe spacing of 0.34 nm, which matched the d-spacing of the (002) atomic layer of graphite. On the outside, there appears to be an amorphous carbon layer surrounding the graphite core. The X-ray diffraction (XRD) spectrum of the nanowires in Figure S6 in the Supporting Information shows a peak at around 26.6° and 45°, which further proves the presence of graphite phase. X-ray photoelectron spectra (XPS) in Figure 2c and Figure S7 (Supporting Information) show that there were C—O (533.1 eV),[15] C=O (531.9 eV),[16] C—Si (102.7 eV),[17] and Si—O (103.5 eV)[17] bonds distributed on the surface of the nanowires. Generally, polar groups like C—O and C=O can facilitate the capturing of PM by near-field interactions.[15,18] The result of thermogravimetric analysis (TGA) in oxygen of the nanowire integrated SS304 mesh is shown in Figure 2d. The sample weight did not change noticeably until the temperature reached 550 °C, suggesting that thermal oxidation of the carbon nanowires was not significant up to this temperature. The sample weight reached a minimum at around 780 °C, and a weight loss of 22% should be close to the mass fraction of the carbon nanowires grown on the SS304 mesh. Typically, carbon materials with a high degree of graphitization are more stable when heated in oxygen.[19] The graphitic component observed in the nanowires is expected to improve the overall heat resistance of the carbon nanowires.

2.2. Growth Mechanism of the Carbon Nanowires on SS304

As observed by TEM, majority of the nanowires contained a high-density particle embedded at a certain location, which

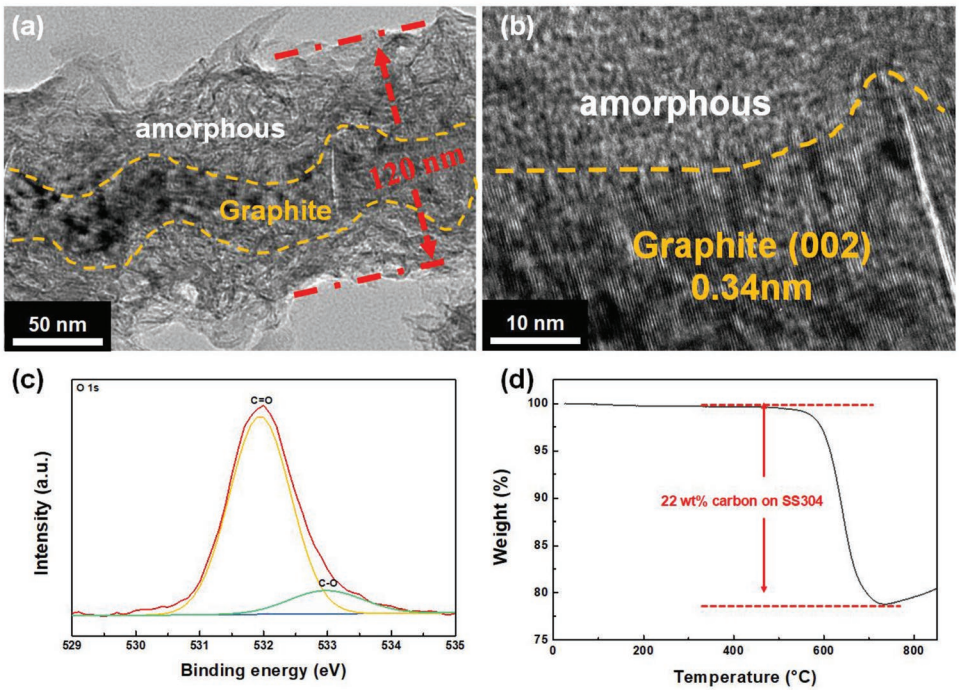

Figure 2. a,b) TEM images of the carbon nanowire; c) XPS O 1s spectrum of the carbon nanowire; d) TGA of the filter tested in O_2.

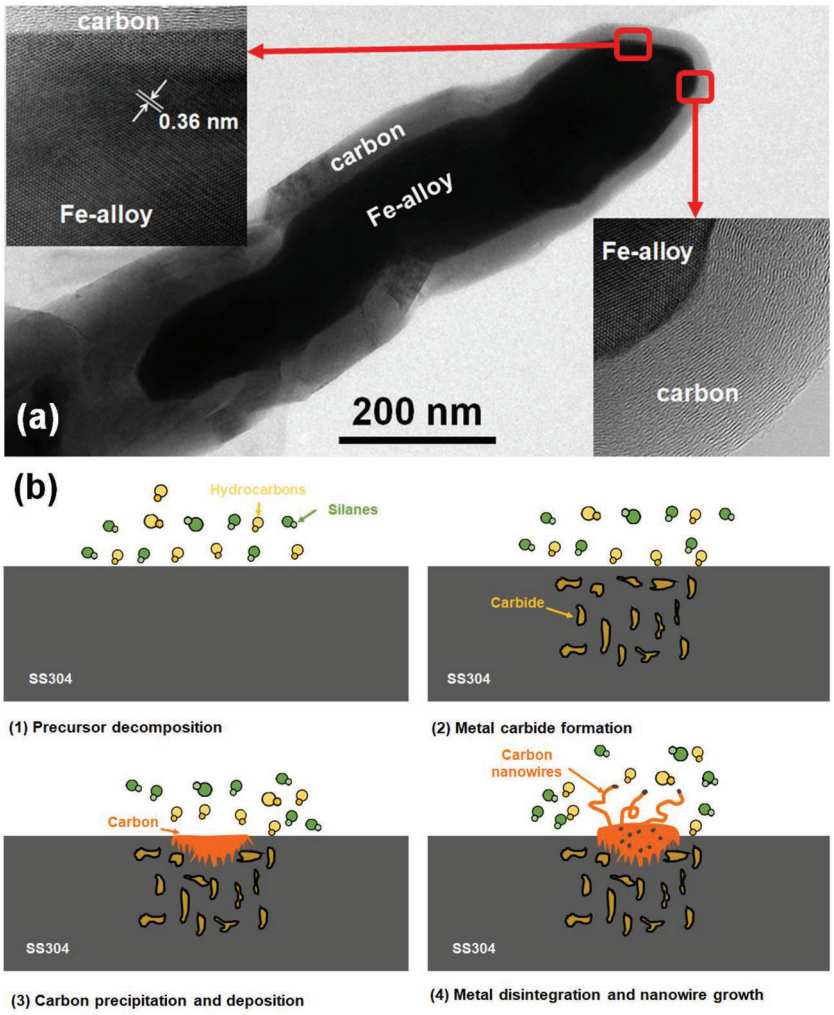

Figure 3. a) TEM images showing the tip of a single carbon nanowire; b) Proposed steps in the growth of the carbon nanowires from bulk SS304.

in most cases near the tip of the nanowire. **Figure 3**a and Figure S8 (Supporting Information) show the details of such particles. As shown in Figure S8 in the Supporting Information, energy dispersive X-ray spectroscopy (EDS) element mapping reveals that the high-density particle contained Fe and Cr of which the distributions largely overlap. HRTEM observation in Figure 3a shows the layered structure of carbon surrounding the particle. As the HRTEM image of the tip in the insets of Figure 3a shows, a fringe spacing of 0.36 nm in the dense particle matches the lattice constant of the face center cubic phase of Fe-alloy austenite. Since the distributions of Fe and Cr largely overlapped within the dense particle as shown in Figure S8 in the Supporting Information, it can be inferred that the dense particle is an alloy of Fe and Cr. The elemental contents of the pretreated SS304 mesh measured by EDS (Table S2 and Figure S9, Supporting Information) found a Fe content of 64 wt% and a Cr content of 17 wt%, which match the nominal composition of SS304. It is likely that the high-density particle directly disintegrated from the bulk SS304 substrate and ended up as the catalyst in the carbon nanowire.

Based on these observations on the structural features, we have proposed a possible mechanism of carbon nanowires growing from the surface of a bulk SS304 substrate. It is a common art to grow vertically aligned carbon nanowires using metallic nanoparticles which catalyze the growth of carbon from gaseous hydrocarbons at an elevated temperature.[20] Usually the metallic nanoparticles can be formed on an inert substrate by deposition of an ultrathin metallic film followed by subsequent heat treatment.

The growth mechanism of the carbon nanowires of our work can be illustrated in Figure 3b. For a bulk SS304 substrate such as the SS304 mesh in this work, formation of metallic nanoparticles is the prerequisite to grow carbon nanowires. Disintegration of SS304 nanoparticles from the bulk SS304 substrate is likely initiated by a carbon-driven corrosion process which is known as "metal dusting."[21] As shown in Figure 3b, in the first stage, the silicone precursor decomposes at a high temperature, and it produces various gaseous hydrocarbons and silanes.[22] The weight loss of the silicone during pyrolysis was about 42% as revealed by TGA in argon (Figure S10, Supporting Information). To better identify the decomposition temperature of the precursor, differential thermal analysis (DTA) curve was derived and shown in Figure S11 (Supporting Information). When the temperature was below 150 °C, the weight loss was mostly caused by removal of moisture and the −OH groups. In the temperature range from 300 °C to about 800 °C, the precursor decomposed to produce a mixture of hydrocarbons and silanes. Although there are four peaks observed in the DTA curve, actual species of the decomposition products cannot be determined without additional analysis. The TGA result suggests that complete decomposition of the precursor requires a temperature of at least 800 °C. In the second stage, in an atmosphere where carbon activity is high, carbon diffuses into the bulk metal and form metastable metal carbides. Next, as more carbon diffuses into the bulk SS304, carbon starts to precipitates out within the bulk SS304 near the surface due to supersaturation. In the final stage, due to the overwhelming internal stress caused by the formation of carbides and precipitation of carbon, both of a lower density than SS304, the bulk alloy near the surface gradually pulverizes and ejects particles. These alloy particles become the catalyst for the growth of a continuous carbon nanowire. Since these alloy particles have been covered in carbon, the growth of other materials such as silica or SiC from these catalytic centers is inhibited. Although the decomposition product of the silicone precursor contains a large content of silanes, which has been previously demonstrated to produce Si-based ceramic nanowires on metal catalysts,[23] only carbon nanowires were produced in this study. The metal dusting process is sensitive to the

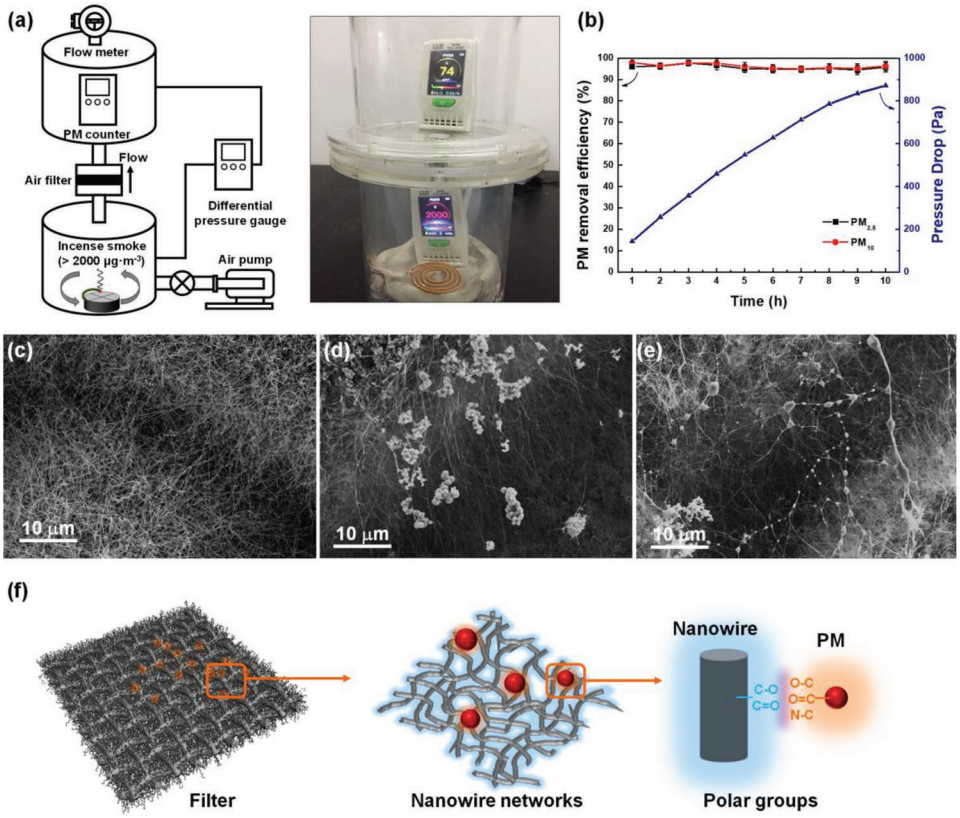

Figure 4. a) Setup for measuring the PM filtration performance; b) PM removal efficiency and pressure drop as a function of time; c) SEM of initial nanowires; d,e) SEM of nanowires after PM capturing; f) PM capturing mechanism at different levels of scales.

temperature and the formation of metal particles is possible only in a certain temperature range. As already shown in Figure S4 in the Supporting Information, when the temperature is too high (1200 °C), SS304 mesh showed obvious deformation and the metallic nanoparticles were likely to sinter and recombine. When the temperature is low (1000 °C), only short nanowires are sparsely grown on SS304.

To further verify the metal dusting phenomenon, a flat SS304 pellet was used as the substrate instead of the stainless steel mesh using the same process for growing carbon nanowires. The surface of the SS304 pellet after the experiment is shown in Figure S12 (Supporting Information). Compared to the smooth surface of the original SS304 pellet, the surface of the SS304 pellet became rough after the nanowire growth experiment and there were dark marks on the surface. There are two typical regions as shown in Figure S12d (Supporting Information) as revealed by SEM. In region 1, loose carbon layer covered the surface. While in region 2, there are some nanowires. The result verified that the SS304 material underwent a metal dusting corrosion under the experimental condition. Additionally, we examined the cross-section of a single metal wire from the SS304 mesh after nanowire growth. As shown in Figure S13a (Supporting Information), the SS304 wire is surrounded by carbon. As shown in Figure S13e (Supporting Information), which is the enlarged region A in Figure S13a (Supporting Information), there are nanoparticles containing Fe and Cr in the carbon-rich region as shown in Figure S13f (Supporting Information).

2.3. PM Filtration Performance

The PM filtration performance was measured using a custom-built setup shown in **Figure 4**a and Figure S14 (Supporting Information). The burning incense coil produced PM containing harmful organic wastes including polycyclic aromatic hydrocarbons (PAHs) and some other hydroxyl compounds which are common organic components in industrial or vehicle gas emissions. The burning rate of the incense coil was stable and repeatable. The chemical composition of the PM produced by the incense coil was analyzed by FTIR and XPS. Polar groups like C−O, C = O, C−N, C−H, and O−H were found in the PM from the burning incense coil (Figure S15, Supporting Information), and these surface groups can interact with the surface groups on the nanowires and effective capturing can be achieved.

Figure 4b shows the PM removal efficiency as a function of time. For $PM_{2.5}$, the removal efficiency during the first hour was 96.1%, and remained virtually unchanged for up to 10 h (96.7% at 10 h). The removal efficiency for PM_{10} was also similar. SEM images of the nanowires before and after filtration are shown in Figure 4c,d,e. Particles with both irregular shapes and droplet-like appearance were observed, suggesting that the nanowires are capable of capturing both solid and likely liquid particles. The initial pressure drop of the filter was typically 200–300 Pa, and the pressure drop gradually increased as a result of the interstitial space within the nanowire networks was filled with PM. A filter relying on the size-effect to stop the passing

of particles will quickly become clogged as the particles fill the pores. In comparison, a nanowire network can catch many particles on collisions while still maintaining many bypasses for gas flow owing to its large void volume.[6,7,15,18] Figure 4f shows the PM capturing mechanism of the filters, owing to the outreaching networks of the nanowires, the particles in the flow will easily collide with one of the nanowires and become attached. The functional groups on the nanowires work as "catchers" to interact with the polar groups on the PM. As the waste gas flow continued, the particles continued to accumulate on the filter.

2.4. Filter Renewal and Cycling Performance

It is required to replace or clean a filter after it is saturated with particles, but the process can be inconvenient and expensive in some scenarios such as aerospace station or complicated industrial machines. Carbon based materials synthesized at high temperatures often show good electrical and thermal conductivity, it is possible to use electrical resistive heating to clean the filters for reuse. As shown in **Figure 5**a, the electrical resistance of the filter increased linearly as temperature increasing during electrical resistive heating. Figure 5b shows the relationship between the heating power and the temperature. These results provide information for determining the electrical resistive heating parameters. TGA tests were carried out in oxygen to find out at what temperature the PM will decompose. As shown in Figure 5c and the differential weight changes in Figure S16 (Supporting Information), the PM particles were nearly completely burnt off at 550 °C while the filter remained quite stable. Temperature of 450 °C was chosen as the heating temperature for the electrical heating renewal treatment and TGA was run at this temperature in O_2. After being heated for 200 min in O_2, the PM was mostly burnt off with 98% weight loss (Figure 5d), while the filter lost only 4% of its initial weight or 20% of the weight of the carbon nanowires. As shown in Figure S17 in the Supporting Information, the weight loss rate of the carbon nanowires in the linear region of the TGA curve was much lower than that of the PM. Although the carbon nanowires were susceptible to oxidation, they are still more stable than PM when being heated. Therefore, an electrical heating process for renewing the filter is possible.

Figure S18b (Supporting Information) shows the SEM image of the filter after the electrical resistive heating renewal treatment (3.1 A and 12.7 W for 180 min). The particles attached on the nanowires were mostly removed as expected compared to the filter right after PM capturing (Figure S18a, Supporting Information). The renewed filter was used for filtering PM again, and the filtration-renewal cycle was repeated to assess the durability of the filter. In each filtration-renewal cycle, the filter was renewed after 10 h PM filtration process, and then was subjected to electrical resistive heating (3.1 A and 12.7 W for 180 min). The PM removal efficiency and pressure drop through multiple cycles are shown in **Figure 6** and summarized in Table S3 (Supporting Information). The average $PM_{2.5}$ removal efficiency was 95.7% for the new filter and it did not change significantly during the first three cycles. After the 3rd renewal process, the efficiency was still above 93.9% which indicated that the filter can be functional for at least four cycles. The $PM_{2.5}$ removal efficiency decreased to 75.6% after the 4th cycle and 52.1% after the 5th cycle, and 30.1% after the 6th cycle. The bare SS304 mesh caused a pressure drop of 102 Pa. After growth of the nanowires, the pressure drop increased to 258 Pa. During the filtration process, the pressure drop gradually increased and it went over 800 Pa after 10 h of filtration as PM built up on the filter. After each renewal treatment, the pressure drop decreased as the accumulated PM was burnt off. If we look at the pressure drop after each renewal treatment, we find that the pressure

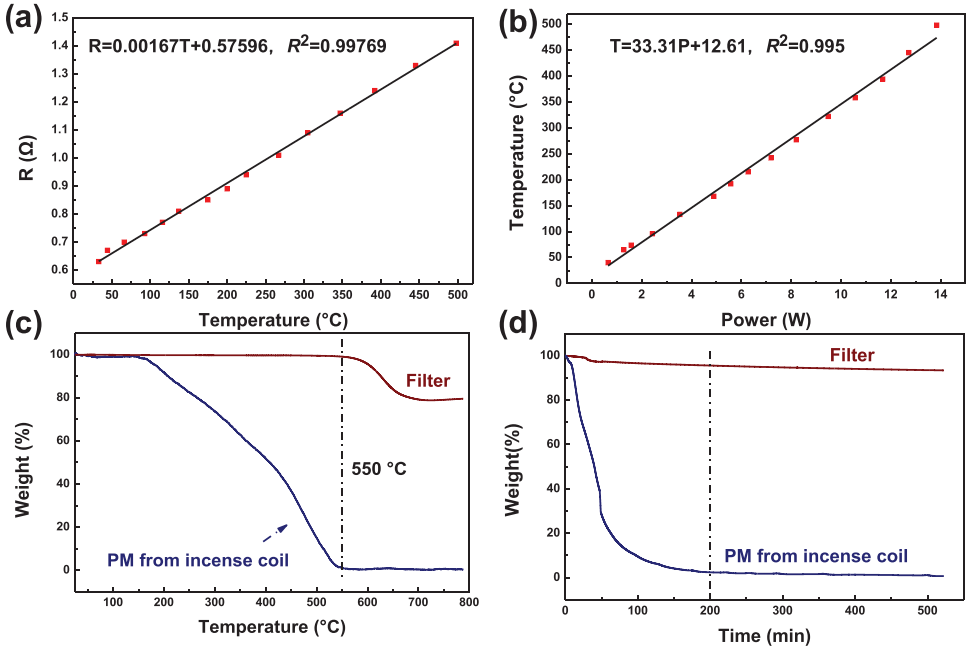

Figure 5. a,b) Electrical heating of the filters; c,d) Thermal oxidation of the filters compared to the PM from incense coil (450 °C in O_2).

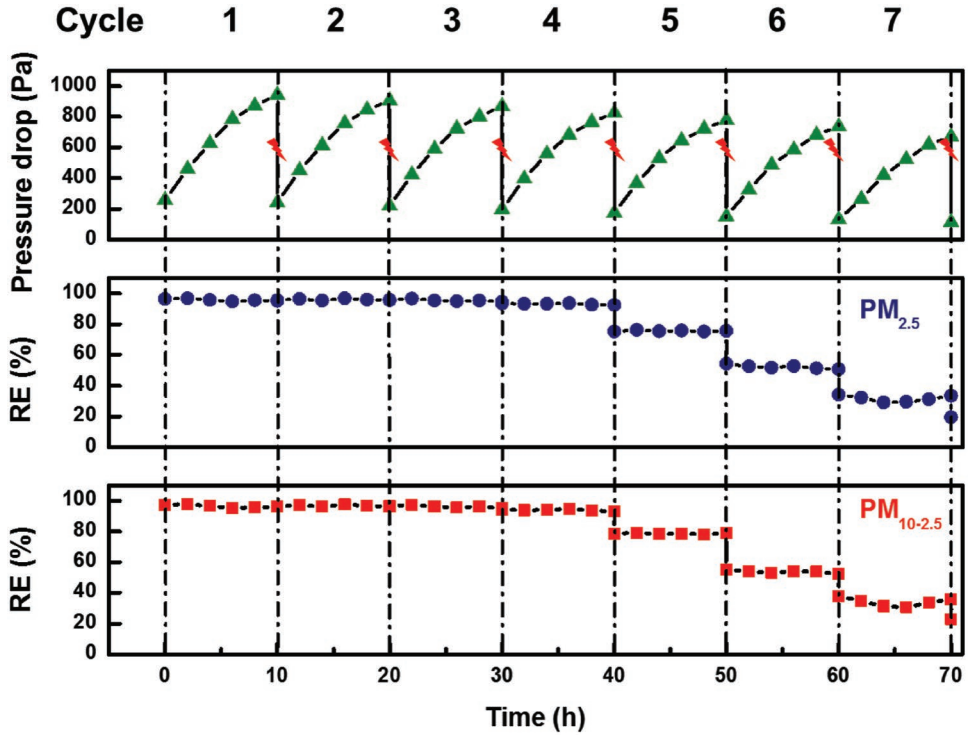

Figure 6. Renewal test of the filter for multiple uses. Electrical heating was applied after every 10 h of PM capturing to renew the filter.

drop of a renewed filter kept decreasing cycle after cycle as shown in Figure S19 (Supporting Information). After the 7th renewal process, the pressure drop has decreased to 114 Pa, and the $PM_{2.5}$ removal efficiency dropped to only 19.6%. Decrease of both the PM removal efficiency and the pressure drop after each renewal suggests that besides PM, part of the carbon nanowires were also burnt off gradually due to the electrical resistive heating. The consumption of the carbon nanowires during the renewal process limits the number of renewal cycles of the filter. Although the electrical resistive heating is confirmed to be effective to renew the filter, it also consumes the carbon nanowires, which are the major effective PM capturer in the filter.

In future work, nanowire networks grown from a more oxidation resistant material such as SiC and SiO_2 will be pursued. Nonetheless, the concept of a PM filter with a robust metal backbone, integrated 3D nanowire networks for effective PM capturing, capability of being electrically renewable, and potentially capable for high temperature gas filtration, is demonstrated in this work, and it can be applied to a vast range of applications including renewable indoor air cleaning as well as particulate filter for diesel engines.

3. Conclusion

In summary, a robust metal-based air filter integrated with 3D carbon nanowires networks was produced and demonstrated. The filter showed a high PM removal efficiency and a low resistance to airflow owing to the unique microstructure and specific functional groups on the nanowires. The carbon nanowire growth mechanism was investigated. Alloy particles containing Fe and Cr first disintegrated from the bulk SS304 and then catalyze the growth of carbon nanowires from the decomposition products of polysiloxane at a high temperature. The filter was thermally stable owing to the graphitic component in the nanowires. Electrical resistive heating strategy to renew the filter after PM filtration was demonstrated. The filter could be renewed to maintain a high PM removal efficiency and low pressure drop for up to four cycles. The microstructure and chemistry of the nanowires could be potentially tunable using different precursors and different synthesis temperature and duration, and the PM removal efficiency and cycling stability can be optimized. Such robust, high efficiency, and renewable air filter is expected to have great potential for treating high temperature and organic waste gas emissions.

4. Experimental Section

Growth of Carbon Nanowires: The preparation of the polysiloxane precursor was by curing of a commercial room temperature vulcanized (RTV) silicone with some modification. In a typical process, 10 g RTV 615A (Momentive) and 1 g ethylene glycol (Aladdin) were mixed in a disposable cup and manually stirred for 10 min to get a homogeneous mixture. Then 15 µL 2 wt% Pt catalyst solution (platinum (0)-1,3-divinyl-1,1,3,3-tetramethyldisiloxane complex solution, Sigma-Aldrich) and 0.5 g PMHS (Sigma-Aldrich) were added and the mixture was stirred for another 5 min. The mixture was left undisturbed at room temperature for 12 h to ensure complete cross-linking to form a silicone elastomer. A 2×2 cm^2 piece of SS304 mesh was sandwiched between two pieces of silicone elastomer, which were cut to a size larger than the SS304 mesh. To avoid adhering of the silicone to the SS304 mesh, a piece of perforated graphite paper was inserted between the silicone and the SS304 mesh (Figure 1a,b). The whole stack was wrapped using a

flexible graphite paper to minimize oxidation of the substrate and the precursor at high temperatures. The wrapped stack was heated to a temperature (1000, 1050, 1100, or 1200 °C) at a ramp rate of 5 °C min^{-1} and maintained at that temperature for 1 h in a tube furnace under argon flow. After cooling down to room temperature, the SS304 mesh was retrieved and used for the following experiments.

Material Characterizations: FTIR spectra of the materials were collected using a PerkinElmer Frontier spectrometer to detect the degree of cross-linking. TGA was performed using a Mettler-Toledo TGA/DSC-1 system. SEM was performed with a ZEISS Supra 55 field emission scanning electron microscope. TEM images were obtained using an FEI TecnaiG2 F30. XPS spectra were obtained to analyze element contents using an ESCALAB 250XL X-ray photoelectron spectrometer.

Measurement of PM Filtration Performance: A twin-chamber cylindrical container was built of acrylic parts for measuring the PM filtration performance. The bottom chamber was used as the PM generator to produce simulated polluted air, the top chamber was used for measuring the filtered air, and the filter was inserted in the flow path connecting these two chambers. In the PM generator, a burning incense coil was used to produce PM, and an electrical fan was used to circulate the PM to achieve a homogeneous PM concentration in the simulated polluted air. An air pump was connected to the bottom chamber and forced a constant airflow through the filter. The particle concentrations upstream and downstream of the filter were measured in situ with a PM particle counter (DT968, sensitivity 1 μg m^{-3}, CEM, China). A differential pressure gauge (GM505, pressure sensitivity 0.3%, time sensitivity 0.5 s, Benetech, China) was used to measure the pressure drop across the filter. The flow rate was measured downstream of the filter using a flow meter (0.5 mL min^{-1}, Senlod, China) and the flow rate was controlled at 2.4 L h^{-1} using a needle valve. The linear airflow velocity was calculated to be 0.1 m s^{-1}. Maintaining a constant flow downstream of the filter was necessary to prevent a false judgment on the functionality of the filter. If a downstream flow was not observed, it can be concluded that the filter was completely filled with particles and the flow path was clogged. In this case, the PM concentration downstream was meaningless and was not recorded. In an experiment, the pressure drop was monitored constantly to avoid complete saturation of the filter. The PM concentration and pressure drop were recorded hourly.

Filter Renewal by Electrical Resistive Heating: Figure S20 (Supporting Information) shows the setup to measure the relationship between the electrical resistance and the temperature of the filter. The temperature was measured using a K-type thermocouple (sensitivity 1 °C, TASI, China), and the current and voltage were measured using a multimeter (sensitivity 0.1 Ω, UNI-T UT603, China). A DC power supply (MAISHENG MS-1520D, China) provided a constant current to heat the filter. The electrical resistance and the heating power of the filter were defined by the following equations

$$R = \frac{U}{I} \tag{1}$$

$$P = UI \tag{2}$$

Where R is the resistance of filter, U is the applied voltage on the filter, P is the heating power, and I is the current through the filter.

Supporting Information

Supporting Information is available from the Wiley Online Library or from the author.

Acknowledgements

K.Y. and Z.Y. contributed equally to this work. This research was financially supported by the Shenzhen Science and Technology Research Grant No. JCYJ20170818085823773, the Guangdong Key-lab Project No. 2017B0303010130, and the National Materials Genome Project (2016YFB0700600).

Conflict of Interest

The authors declare no conflict of interest.

Keywords

carbon nanowire, metal dusting, renewable PM filter, stainless steel substrate

Received: January 30, 2019
Revised: February 27, 2019
Published online: April 3, 2019

[1] a) I. Kloog, F. Nordio, B. A. Coull, J. Schwartz, *Environ. Sci. Technol.* **2012**, *46*, 11913; b) C. J. Lee, R. V. Martin, D. K. Henze, M. Brauer, A. Cohen, A. v. Donkelaar, *Environ. Sci. Technol.* **2015**, *49*, 4335.
[2] a) J. O. Anderson, J. G. Thundiyil, A. Stolbach, *J. Med. Toxicol.* **2012**, *8*, 166; b) N. Li, C. Sioutas, A. Cho, D. Schmitz, C. Misra, J. Sempf, M. Wang, T. Oberley, J. Froines, A. Nel, *Environ. Health Perspect.* **2003**, *111*, 455; c) D. J. Nowak, S. Hirabayashi, A. Bodine, R. Hoehn, *Environ. Pollut.* **2013**, *178*, 395.
[3] C.-s. Wang, Y. Otani, *Ind. Eng. Chem. Res.* **2013**, *52*, 5.
[4] P. Li, C. Wang, Y. Zhang, F. Wei, *Small* **2014**, *10*, 4543.
[5] a) P. Li, Y. Zong, Y. Zhang, M. Yang, R. Zhang, S. Li, F. Wei, *Nanoscale* **2013**, *5*, 3367; b) S. J. Park, D. G. Lee, *Carbon* **2006**, *44*, 1930; c) G. Viswanathan, D. B. Kane, P. J. Lipowicz, *Adv. Mater.* **2004**, *16*, 2045.
[6] R. Zhang, C. Liu, P.-C. Hsu, C. Zhang, N. Liu, J. Zhang, H. R. Lee, Y. Lu, Y. Qiu, S. Chu, Y. Cui, *Nano Lett.* **2016**, *16*, 3642.
[7] C. Wang, S. Wu, M. Jian, J. Xie, L. Xu, X. Yang, Q. Zheng, Y. Zhang, *Nano Res.* **2016**, *9*, 2590.
[8] K. Desai, K. Kit, J. Li, P. Michael Davidson, S. Zivanovic, H. Meyer, *Polymer* **2009**, *50*, 3661.
[9] J. Xiao, J. Liang, C. Zhang, Y. Tao, G.-W. Ling, Q.-H. Yang, *Small Methods* **2018**, *2*, 1800012.
[10] C.-S. Wang, *Powder Technol.* **2001**, *118*, 166.
[11] a) R. Betha, S. N. Behera, R. Balasubramanian, *Environ. Sci. Technol.* **2014**, *48*, 4327; b) Z. Cheng, J. Jiang, O. Fajardo, S. Wang, J. Hao, *Atmos. Environ.* **2013**, *65*, 186; c) R.-J. Huang, Y. Zhang, C. Bozzetti, K.-F. Ho, J.-J. Cao, Y. Han, K. R. Daellenbach, J. G. Slowik, S. M. Platt, F. Canonaco, P. Zotter, R. Wolf, S. M. Pieber, E. A. Bruns, M. Crippa, G. Ciarelli, A. Piazzalunga, M. Schwikowski, G. Abbaszade, J. Schnelle-Kreis, R. Zimmermann, Z. An, S. Szidat, U. Baltensperger, I. E. Haddad, A. S. H. Prévôt, *Nature* **2014**, *514*, 218; d) L. Ma, H. Verelst, G. V. Baron, *Catal. Today* **2005**, *105*, 729; e) A. Thorpe, R. M. Harrison, *Sci. Total Environ.* **2008**, *400*, 270; f) S. Zhao, L. Chen, Y. Li, Z. Xing, K. Du, *Atmosphere* **2015**, *6*, 234.
[12] a) A. Zanoletti, F. Bilo, L. Borgese, L. E. Depero, A. Fahimi, J. Ponti, A. Valsesia, R. La Spina, T. Montini, E. Bontempi, *Front. Chem.* **2018**, *6*, 534; b) A. Zanoletti, F. Bilo, L. E. Depero, D. Zappa, E. Bontempi, *J. Environ. Manage.* **2018**, *218*, 355.
[13] M. Wójcik-Bania, A. Łącz, A. Nyczyk-Malinowska, M. Hasik, *Polymer* **2017**, *130*, 170.
[14] O. O. Sonibare, T. Haeger, S. F. Foley, *Energy* **2010**, *35*, 5347.
[15] C. Liu, P.-C. Hsu, H.-W. Lee, M. Ye, G. Zheng, N. Liu, W. Li, Y. Cui, *Nat. Commun.* **2015**, *6*, 6205.
[16] T. Asakawa, K. Tanaka, I. Toyoshima, *Langmuir* **1988**, *4*, 521.

[17] M. Halim, C. Hudaya, A. Y. Kim, J. K. Lee, *J. Mater. Chem. A* **2016**, *4*, 2651.
[18] B. Khalid, X. Bai, H. Wei, Y. Huang, H. Wu, Y. Cui, *Nano Lett.* **2017**, *17*, 1140.
[19] a) W. H. Awad, C. A. Wilkie, *Polymer* **2010**, *51*, 2277; b) C. Chen, K. Liu, H. Wang, W. Liu, H. Zhang, *Sol. Energy Mater. Sol. Cells* **2013**, *117*, 372; c) F. d. C. Fim, N. R. S. Basso, A. P. Graebin, D. S. Azambuja, G. B. Galland, *J. Appl. Polym. Sci.* **2013**, *128*, 2630; d) T. Cui, P. Li, Y. Liu, J. Feng, M. Xu, M. Wang, *Mater. Chem. Phys.* **2012**, *134*, 1160.
[20] a) M. Chhowalla, K. B. K. Teo, C. Ducati, N. L. Rupesinghe, G. A. J. Amaratunga, A. C. Ferrari, D. Roy, J. Robertson, W. I. Milne, *J. Appl. Phys.* **2001**, *90*, 5308; b) Y. Murakami, S. Chiashi, Y. Miyauchi, M. Hu, M. Ogura, T. Okubo, S. Maruyama, *Chem. Phys. Lett.* **2004**, *385*, 298; c) Z. F. Ren, Z. P. Huang, J. W. Xu, J. H. Wang, P. Bush, M. P. Siegal, P. N. Provencio, *Science* **1998**, *282*, 1105.
[21] C. M. Chun, T. A. Ramanarayanan, *J. Electrochem. Soc.* **2005**, *152*, B169.
[22] a) N. Grassie, I. G. Macfarlane, *Eur. Polym. J.* **1978**, *14*, 875; b) E. Radovanovic, M. F. Gozzi, M. C. Gonçalves, I. V. P. Yoshida, *J. Non-Cryst. Solids* **1999**, *248*, 37; c) M. A. Schiavon, S. U. A. Redondo, S. R. O. Pina, I. V. P. Yoshida, *J. Non-Cryst. Solids* **2002**, *304*, 92; d) T. H. Thomas, T. C. Kendrick, *J. Polym. Sci., Part A-2* **1969**, *7*, 537; e) Z. Yang, L. Feng, S. Diao, S. Feng, C. Zhang, *Thermochim. Acta* **2011**, *521*, 170.
[23] a) M. Fukushima, Y.-i. Yoshizawa, P. Colombo, *J. Am. Ceram. Soc.* **2012**, *95*, 3071; b) C. Vakifahmetoglu, E. Pippel, J. Woltersdorf, P. Colombo, *J. Am. Ceram. Soc.* **2010**, *93*, 959.